



1           **Moment-based Metrics for Global Sensitivity Analysis of Hydrological Systems**

2

3                           Aronne Dell'Oca<sup>1</sup>, Monica Riva<sup>1,2</sup>, Alberto Guadagnini<sup>1,2</sup>

4

5           <sup>1</sup>Dipartimento di Ingegneria Civile e Ambientale (DICA), Politecnico di Milano, Piazza L. Da

6   Vinci, 32, 20133 Milano, Italy

7           <sup>2</sup>Department of Hydrology and Atmospheric Sciences, University of Arizona, Tucson, Arizona,

8   USA



9

## Abstract

10 We propose new metrics to assist global sensitivity analysis, GSA, of hydrological and Earth  
11 systems. Our approach allows assessing the impact of uncertain parameters on main features of the  
12 probability density function, pdf, of a target model output,  $y$ . These include the expected value of  $y$ ,  
13 the spread around the mean and the degree of symmetry and tailedness of the pdf of  $y$ . Since reliable  
14 assessment of higher order statistical moments can be computationally demanding, we couple our  
15 GSA approach with a surrogate model, approximating the full model response at a reduced  
16 computational cost. Here, we consider the generalized Polynomial Chaos Expansion (gPCE), other  
17 model reduction techniques being fully compatible with our theoretical framework. We demonstrate  
18 our approach through three test cases, including an analytical benchmark, a simplified scenario  
19 mimicking pumping in a coastal aquifer, and a laboratory-scale conservative transport experiment.  
20 Our results allow ascertaining which parameters can impact some moments of the model output pdf  
21 while being uninfluential to others. We also investigate the error associated with the evaluation of our  
22 sensitivity metrics by replacing the original system model through a gPCE. Our results indicate that  
23 the construction of a surrogate model with increasing level of accuracy might be required depending  
24 on the statistical moment considered in the GSA. Our approach is fully compatible with (and can  
25 assist the development of) analysis techniques employed in the context of reduction of model  
26 complexity, model calibration, design of experiment, uncertainty quantification and risk assessment.

27



## 1. Introduction

Our improved understanding of physical-chemical mechanisms governing hydrological processes at multiple space and time scales and the ever increasing power of modern computational resources are at the heart of the formulation of conceptual models which are frequently characterized by marked levels of sophistication and complexity. This is evident when one considers the spectrum of mathematical formulations and ensuing level of model parametrization rendering our conceptual understanding of given environmental scenarios (Grauso et al., 2007; Wagener and Montanari, 2011; Koutsoyiannis, 2010; Wagener et al., 2010; Paniconi and Putti, 2015; Hartmann et al., 2013; Herman et al., 2013; Willmann et al., 2006; Elshorbagy et al., 2010a,b; Förster et al., 2014). Model complexity can in turn exacerbate challenges associated with the need to quantify the way uncertainties associated with parameters of a given model propagate to target state variables.

In this context, approaches based on rigorous sensitivity analysis are valuable tools to improve our ability to (i) quantify uncertainty, (ii) enhance our understanding of the relationships between model input and outputs, and (iii) tackle the challenges of model- and data- driven design of experiments. These also offer insights to guide model simplification, e.g., by identifying model input parameters that have negligible effects on a target output. The variety of available sensitivity methodologies can be roughly subdivided into two broad categories, i.e., local and global approaches. Local sensitivity analyses consider the variation of a model output against variations of model input solely in the neighbourhood of a given set of parameters values. Otherwise, global sensitivity analysis (GSA) quantifies model sensitivity across the complete support within which model parameters can vary. Error measurements and/or lack of knowledge about parameters can be naturally accommodated in a GSA by specifying appropriate parameter intervals and evaluating sensitivity over the complete parameter space. Recent studies and reviews on available sensitivity analysis and approaches are offered by, e.g., Pianosi et al. (2016), Sarrazin et al. (2016), and Razavi and Gupta (2015).

Our study is framed in the context of GSA methods. A broadly recognized strategy to quantify global sensitivity of uncertain model parameters to model outputs relies on the evaluation of the



54 Sobol' indices (Sobol, 1993). These are typically referred to as variance-based sensitivity measures  
55 because the output variance is taken as the metric upon which sensitivity is quantified. A key  
56 limitation of a variance-based GSA is that the uncertainty of the output is implicitly considered to be  
57 fully characterized by its variance. Relying solely on this criterion can provide an incomplete picture  
58 of a system response to model parameters, also considering that probability densities of typical  
59 hydrological quantities can be characterized by highly skewed and tailed distributions (e.g.,  
60 Borgonovo, 2011). Recent studies (e.g., Krykacz-Hausmann, 2001; Borgonovo, 2007) introduce a  
61 sensitivity metric grounded on the complete probability density function, pdf, of the model output.  
62 These so-called moment-independent analyses may suffer from operational constraints, because a  
63 robust evaluation of the complete pdf may require a number of model runs which is computationally  
64 unaffordable. The PAWN method developed by Pianosi and Wagener (2015) attempts to overcome  
65 this limitation introducing a sensitivity metric based on the cumulative density function, which can  
66 potentially be estimated more robustly than its associated pdf for a given sample size.

67       It is clear that while a variance-based GSA can be favored for its conceptual simplicity and  
68 ease of implementation and variance can be considered in some cases as an adequate proxy of the  
69 spread around the mean, it does not yield a forthright quantification of the way variations of a  
70 parameter can affect the structure of the pdf of a target model output. Otherwise, moment-independent  
71 methodologies condense the entire pdf in only one index, somehow clouding our understanding of  
72 how the structure of the pdf is affected by variations of each uncertain model parameter. Here, our  
73 distinctive objective is to contribute to bridge the gap between these two types of GSA. We do so by  
74 introducing theoretical elements and an implementation strategy which enable us to appraise  
75 parameter sensitivity through the joint use of sensitivity indices based on four (statistical) moments  
76 of the pdf of the model output: expected value, variance, skewness and kurtosis. The key idea at the  
77 basis of this strategy is that linking parameter sensitivity to multiple statistical moments leads to  
78 improved understanding of the way a given uncertain parameter can govern key features of the shape



79 of the pdf of desired model outputs, which is of interest in modern applications of hydrological and  
80 Earth sciences.

81 Variance-based GSA has also been applied (*a*) to guide reduction of model complexity, e.g.,  
82 by setting the value of a parameter which is deemed as uninfluential to the variance of a target model  
83 output (e.g., Fu et al., 2012; Chu et al., 2015; Punzo et al., 2015), and (*b*) in the context of uncertainty  
84 quantification (Saltelli et al., 2008; Pianosi et al., 2016; Colombo et al., 2016). Only limited attention  
85 has been devoted to assess the relative effects of uncertain model parameters to the expected value of  
86 the target model output. This information would complement a model complexity analysis by  
87 introducing a quantification of the impact that conditioning the process on prescribed parameter  
88 values would have on the expected value of the output. As stated above, our approach is based on the  
89 joint use of multiple (statistical) moments for GSA. It enables us to address the following critical  
90 questions: When can the variance be considered as a reliable proxy for characterizing model output  
91 uncertainty? Which model parameter mostly affects asymmetry and/or the tailing behavior of a model  
92 output pdf? Does a given model parameter have a marked role in controlling some of the first four  
93 statistical moments of the model output, while being uninfluential to others?

94 Even as the richness of information content that a GSA grounded on the first four statistical  
95 moments might carry can be a significant added value to our system understanding, it may sometimes  
96 be challenging to obtain robust and stable evaluation of the proposed metrics for complex and  
97 computationally demanding models. This can be especially true when considering higher-order  
98 moments such as skewness and kurtosis. To overcome this difficulty, we cast the problem within a  
99 computationally tractable framework by relying on the use of surrogate models, which mimic the full  
100 model response with a reduced computational burden. Amongst the diverse available techniques to  
101 construct a surrogate model (see, e.g., Razavi et al., 2012a,b), we exemplify our approach by  
102 considering the generalized Polynomial Chaos Expansion (gPCE) that has been successfully applied  
103 to a variety complex environmental problems (Sudret, 2008; Ciriello et al., 2013; Formaggia et al.,  
104 2013; Riva et al., 2015; Gläser et al., 2016), other model reduction techniques being fully compatible



with our GSA framework. In this context, we also investigate the error associated with the evaluation of the sensitivity metrics we propose by replacing the original (full) system model through the selected surrogate model for three test cases. These include a widely employed analytical benchmark, a pumping scenario in a coastal aquifers, and a laboratory-scale transport setting. The remainder of the work is organized as follows. Section 2 presents our theoretical framework and developments. Section 3 illustrates our results for the three test cases indicated above and conclusions are drawn in Sect. 4.

## 2. Theoretical framework

We start by recalling the widely used variance-based GSA metrics in Sect. 2.1. These allow quantifying the contribution of each uncertain parameter to the total variance of a state variable of interest. We also provide a brief overview of the generalized Polynomial Chaos Expansion (gPCE) technique, which we use to construct a surrogate of the full system model. We then illustrate in Sect. 2.2 the theoretical developments underlying our approach and introduce novel GSA indices.

### 2.1 Sobol' indices for variance-based GSA and generalized Polynomial Chaos Expansion

We consider a target system state variable,  $y$ , which depends on  $N$  random parameters. These are collected in vector  $\mathbf{x} = (x_1, x_2, \dots, x_N)$  and defined in the parameter space  $\Gamma = \Gamma_1 \times \Gamma_2 \times \dots \times \Gamma_N$ ,  $\Gamma_i = [x_{i,\min}, x_{i,\max}]$  being the support of the  $i$ -th random variable  $x_i$ . Variance-based GSA approaches consider variance as the sole metric to quantify the contribution of each uncertain parameter to the uncertainty of  $y$ . Iman and Hora (1990) introduce the following index

$$HI_{x_i} = V[y] - E[V[y | x_i]] = V[E[y | x_i]], \quad (1)$$

$E[-]$  and  $V[-]$  respectively denoting expectation and variance operators. Index  $HI_{x_i}$  quantifies the expected reduction of variance due to knowledge of  $x_i$  (the symbol  $|x_i$  in Eq. (1) indicates conditioning on  $x_i$ ). A similar measure is offered by the widely used Sobol' indices (Sobol, 1993). These have been defined starting from the Hoeffding/Sobol decomposition (see, e.g., Sobol, 1993, Le Maître and Knio, 2010) of  $y(\mathbf{x})$  when  $\mathbf{x}$  is a collection of independent random variables as



$$y(\mathbf{x}) = y_0 + \sum_{x_i=1}^N y_{x_i}(x_i) + \sum_{x_i < x_j} y_{x_i, x_j}(x_i, x_j) + \dots + y_{x_1, x_2, \dots, x_N}(x_1, x_2, \dots, x_N), \quad (2)$$

where

$$\begin{aligned} y_0 &= \int_{\Gamma} y(\mathbf{x}) \rho_{\Gamma \mathbf{x}} d\mathbf{x}, \\ y_{x_i}(x_i) &= \int_{\Gamma \sim x_i} y(\mathbf{x}) \rho_{\Gamma \sim x_i} d\mathbf{x}_{\sim x_i} - y_0, \\ y_{x_i, x_j}(x_i, x_j) &= \int_{\Gamma \sim x_i, x_j} y(\mathbf{x}) \rho_{\Gamma \sim x_i, x_j} d\mathbf{x}_{\sim x_i, x_j} - y_{x_i}(x_i) - y_{x_j}(x_j) - y_0, \end{aligned} \quad (3)$$

and so on,  $\rho_{\Gamma \mathbf{x}}$  being the pdf of  $\mathbf{x}$ . The integral  $\int_{\Gamma \sim x_i} y(\mathbf{x}) \rho_{\Gamma \sim x_i} d\mathbf{x}_{\sim x_i}$  in Eq. (3) represents integration

of  $y(\mathbf{x})$  over the space of all entries of vector  $\mathbf{x}$  excluding  $x_i$ ,  $\rho_{\Gamma \sim x_i}$  being the corresponding pdf. The

Sobol' index  $S_{x_{i_1}, x_{i_2}, \dots, x_{i_s}}$  is associated with the mixed effect of  $x_{i_1}, x_{i_2}, \dots, x_{i_s}$  on the variance of  $y(\mathbf{x})$ ,

$V[y]$ , and can be computed as

$$S_{x_{i_1}, x_{i_2}, \dots, x_{i_s}} = \frac{1}{V[y]} \int_{\Gamma_{x_{i_1}, x_{i_2}, \dots, x_{i_s}}} y_{x_{i_1}, x_{i_2}, \dots, x_{i_s}}(x_{i_1}, x_{i_2}, \dots, x_{i_s}) \rho_{\Gamma_{x_{i_1}, x_{i_2}, \dots, x_{i_s}}} dx_{i_1} \dots dx_{i_s}. \quad (4)$$

The principal and total Sobol' indices are respectively defined as

$$S_{x_i} = \frac{1}{V[y]} \int_{\Gamma_{x_i}} [y_{x_i}(x_i)]^2 \rho_{\Gamma_{x_i}} dx_i, \quad (5)$$

$$S_{x_i}^T = S_{x_i} + \sum_{x_j} S_{x_i, x_j} + \sum_{x_j, x_k} S_{x_i, x_j, x_k} + \dots \quad (6)$$

Note that  $S_{x_i}$  describes the relative contribution to  $V[y]$  due to variability of only  $x_i$ . Otherwise,  $S_{x_i}^T$

quantifies the total contribution of  $x_i$  to  $V[y]$ , including all terms where  $x_i$  appears. In other words,

$S_{x_i}^T$  also includes interactions between  $x_i$  and the remaining uncertain parameters, collected in vector

$\mathbf{x}_{\sim x_i}$ . Note that according to Eq.s (1)-(2) and Eq. (5)

$$S_{x_i} = \frac{V[E[y | x_i]]}{V[y]} = \frac{HI_{x_i}}{V[y]}, \quad (7)$$



i.e., the principal Sobol' index represents the relative expected reduction of process variance due to knowledge of (or conditioning on) a parameter. Sobol' indices are commonly evaluated via Monte Carlo quadrature schemes that can be markedly demanding in terms of computational time, especially for complex and highly non-linear settings. Relying on a generalized Polynomial Chaos Expansion, gPCE, as a surrogate of the full mathematical model of the system (Ghanem and Spanos, 1991; Xiu and Karniadakis, 2002; Le Maitre and Knio, 2010; Formaggia et al., 2013; Ciriello et al., 2013; Riva et al., 2015) allows reducing the computational burden associated with GSA techniques. The process  $y(\mathbf{x})$  is represented as a linear combination of multivariate polynomials,  $\psi_p(\mathbf{x})$ , i.e.,

$$y(\mathbf{x}) \approx \beta_0 + \sum_{i=1}^N \sum_{p \in \mathfrak{I}_i} \beta_p \psi_p(\mathbf{x}) + \sum_{i=1}^N \sum_{j=1}^N \sum_{p \in \mathfrak{I}_{i,j}} \beta_p \psi_p(\mathbf{x}) + \dots, \quad (8)$$

$$\psi_p(\mathbf{x}) = \prod_{i=1}^N \psi_{i,p_i}(x_i), \quad \beta_p = \int_{\Gamma} y(\mathbf{x}) \psi_p(\mathbf{x}) \rho_{\Gamma} d\mathbf{x},$$

where  $\mathbf{p} = \{p_1, \dots, p_N\} \in \mathbb{N}^N$  is a multi-index expressing the degree of each univariate polynomial,  $\psi_{i,p_i}(x_i)$ ;  $\beta_p$  are the gPCE coefficients;  $\mathfrak{I}_i$  contains all indices such that only the  $i$ -th component does not vanish;  $\mathfrak{I}_{i,j}$  contains all indices such that only the  $i$ -th and  $j$ -th components are not zero, and so on. Note that  $\beta_0 \equiv y_0$ , i.e.,  $\beta_0$  is the unconditional mean of  $y(\mathbf{x})$ . Finally, the Sobol' indices Eq.s (4)-(5) and the variance of  $y(\mathbf{x})$  can be computed from Eq. (8) as

$$S_{x_{i_1}, \dots, x_{i_s}} = \frac{1}{V[y]} \sum_{p \in \mathfrak{I}_{i_1, \dots, i_s}} \beta_p^2, \quad S_{x_i} = \frac{1}{V[y]} \sum_{p \in \mathfrak{I}_i} \beta_p^2, \quad V[y] = \sum_{p \in \mathbb{N}^N} \beta_p^2 - \beta_0^2. \quad (9)$$

## 2.2 New metrics for multiple-moment GSA

We introduce new metrics to quantify the expected relative change of main features of the pdf of  $y$  due to variability of model input parameters. In contrast with traditional variance-based GSA techniques of the kind described in Sect. 2.1, we quantify changes in the pdf of  $y$  through its first four statistical moments, i.e., mean,  $E[y]$ , variance,  $V[y]$ , skewness,  $\gamma[y]$ , and kurtosis,  $k[y]$ . The latter is an indicator of the behavior of the tails of the pdf of  $y$  and is particularly useful in the context of risk analysis,  $\gamma[y]$  quantifying the asymmetry of the pdf of  $y$ .





168 The effect of changes of  $x$  on the mean of  $y$  cannot be systematically analyzed by the metrics  
 169 currently available in the literature. We therefore introduce the following quantity

$$170 \quad AMAE_{x_i} = \begin{cases} \frac{1}{|y_0|} \int_{\Gamma_{x_i}} |y_0 - E[y | x_i]| \rho_{\Gamma_{x_i}} dx_i = \frac{1}{|y_0|} E[|y_0 - E[y | x_i]|] & \text{if } y_0 \neq 0 \\ \int_{\Gamma_{x_i}} |E[y | x_i]| \rho_{\Gamma_{x_i}} dx_i = E[|E[y | x_i]|] & \text{if } y_0 = 0 \end{cases}, \quad (10)$$

171  $y_0$  being defined in Eq. (3). Extension of Eq. (10) to consider the joint effect of  $x_{i_1}, x_{i_2}, \dots, x_{i_s}$  on the  
 172 mean of  $y$  is straightforward, leading to the following index

$$173 \quad AMAE_{x_{i_1}, \dots, x_{i_s}} = \begin{cases} \frac{1}{|y_0|} \int_{\Gamma_{x_{i_1}, \dots, x_{i_s}}} |y_0 - E[y | x_{i_1}, \dots, x_{i_s}]| \rho_{\Gamma_{x_{i_1}, \dots, x_{i_s}}} dx_{i_1} \dots dx_{i_s} \\ \quad = \frac{1}{|y_0|} E[|y_0 - E[y | x_{i_1}, \dots, x_{i_s}]|] & \text{if } y_0 \neq 0 \\ \int_{\Gamma_{x_{i_1}, \dots, x_{i_s}}} |E[y | x_{i_1}, \dots, x_{i_s}]| \rho_{\Gamma_{x_{i_1}, \dots, x_{i_s}}} dx_{i_1} \dots dx_{i_s} = E[|E[y | x_{i_1}, \dots, x_{i_s}]|] & \text{if } y_0 = 0 \end{cases} \quad (11)$$

174 Note that index  $AMAE_{x_i}$  quantifies the expected relative variation of the mean of  $y$  due to variations  
 175 of only  $x_i$ , while  $AMAE_{x_{i_1}, \dots, x_{i_s}}$  also includes all interactions amongst parameters  $x_{i_1}, x_{i_2}, \dots, x_{i_s}$ .

176 Along the same lines, we introduce the following index

$$177 \quad AMAV_{x_i} = \frac{1}{V[y]} \int_{\Gamma_{x_i}} |V[y] - V[y | x_i]| \rho_{\Gamma_{x_i}} dx_i = \frac{E[|V[y] - V[y | x_i]|]}{V[y]}, \quad (12)$$

178 quantifying the relative expected discrepancy between unconditional and conditional (on  $x_i$ ) process  
 179 variance. Note that Eq. (12) does not generally coincide with the principal Sobol' index  $S_{x_i}$  in Eq.  
 180 (7) that quantifies the expected relative reduction of the variance due to knowledge of  $x_i$  (or, in other  
 181 words, the relative contribution to the variance arising from uncertainty in  $x_i$ ). Index  $AMAV_{x_i}$   
 182 reduces to  $S_{x_i}$  only if the conditional variance,  $V[y | x_i]$ , is always (i.e., for each value of  $x_i$ ) smaller  
 183 than (or equal to) its unconditional counterpart  $V[y]$ . The difference between  $AMAV_{x_i}$  and  $S_{x_i}$ , as



well as advantages of using  $AMAV_{x_i}$ , will be elucidated through the numerical examples illustrated in Sect. 3. Extension of Eq. (12) to consider the joint effect of  $x_{i_1}, x_{i_2}, \dots, x_{i_s}$  reads

$$AMAV_{x_{i_1}, \dots, x_{i_s}} = \frac{1}{V[y]} \int_{\Gamma_{x_{i_1}, \dots, x_{i_s}}} |V[y] - V[y | x_{i_1}, \dots, x_{i_s}]| \rho_{\Gamma_{x_{i_1}, \dots, x_{i_s}}} dx_{i_1} \dots dx_{i_s} \\ = \frac{1}{V[y]} E[|V[y] - V[y | x_{i_1}, \dots, x_{i_s}]|] \quad (13)$$

Index  $AMAV_{x_{i_1}, \dots, x_{i_s}}$  quantifies the expected relative discrepancy between  $V[y]$  and the variance of the process conditional to joint knowledge of  $x_{i_1}, x_{i_2}, \dots, x_{i_s}$ .

We then quantify the relative expected discrepancy between unconditional,  $\gamma[y]$ , and conditional,  $\gamma[y | x_i]$ , skewness through the index

$$AMAG_{x_i} = \begin{cases} \frac{1}{|\gamma[y]|} \int_{\Gamma_{x_i}} |\gamma[y] - \gamma[y | x_i]| \rho_{\Gamma_{x_i}} dx_i = \frac{1}{|\gamma[y]|} E[|\gamma[y] - \gamma[y | x_i]|] & \text{if } \gamma_y \neq 0 \\ \int_{\Gamma_{x_i}} |\gamma[y | x_i]| \rho_{\Gamma_{x_i}} dx_i = E[|\gamma[y | x_i]|] & \text{if } \gamma_y = 0 \end{cases} \quad (14)$$

Extension of Eq. (14) to consider the joint effect of  $x_{i_1}, x_{i_2}, \dots, x_{i_s}$  gives

$$AMAG_{x_{i_1}, \dots, x_{i_s}} = \begin{cases} \frac{1}{|\gamma[y]|} \int_{\Gamma_{x_{i_1}, \dots, x_{i_s}}} |\gamma[y] - \gamma[y | x_{i_1}, \dots, x_{i_s}]| \rho_{\Gamma_{x_{i_1}, \dots, x_{i_s}}} dx_{i_1} \dots dx_{i_s} \\ = \frac{1}{|\gamma[y]|} E[|\gamma[y] - \gamma[y | x_{i_1}, \dots, x_{i_s}]|] & \text{if } \gamma[y] \neq 0 \\ \int_{\Gamma_{x_{i_1}, \dots, x_{i_s}}} |\gamma[y | x_{i_1}, \dots, x_{i_s}]| \rho_{\Gamma_{x_{i_1}, \dots, x_{i_s}}} dx_{i_1} \dots dx_{i_s} = E[|\gamma[y | x_{i_1}, \dots, x_{i_s}]|] & \text{if } \gamma[y] = 0 \end{cases} \quad (15)$$

The relative variation of the kurtosis of  $y$  due to variations of a parameter  $x_i$  or of the parameter set  $x_{i_1}, x_{i_2}, \dots, x_{i_s}$  can be respectively quantified through

$$AMAK_{x_i} = \frac{1}{k[y]} \int_{\Gamma_{x_i}} |k[y] - k[y | x_i]| \rho_{\Gamma_{x_i}} dx_i = \frac{1}{k[y]} E[|k[y] - k[y | x_i]|], \quad (16)$$



$$\begin{aligned}
 197 \quad AMAk_{x_{i_1}, \dots, x_{i_s}} &= \frac{1}{k[y]} \int_{\Gamma_{x_{i_1}, \dots, x_{i_s}}} |k[y] - k[y | x_{i_1}, \dots, x_{i_s}]| \rho_{\Gamma_{x_{i_1}, \dots, x_{i_s}}} dx_{i_1} \dots dx_{i_s} \\
 &= \frac{1}{k[y]} E \left[ |k[y] - k[y | x_{i_1}, \dots, x_{i_s}]| \right]
 \end{aligned} \tag{17}$$

198 Relying jointly on Eq.s (10)-(17) enables one to perform a comprehensive GSA of the target  
 199 process  $y(\mathbf{x})$  quantifying the impact of  $\mathbf{x}$  on the first four (statistical) moments of the pdf of  $y(\mathbf{x})$ .  
 200 This strategy yields information about the way important elements of the distribution of  $y(\mathbf{x})$ , such  
 201 as mean, spread around the mean, symmetry, and tailedness, are affected by model uncertain  
 202 parameters collected in  $\mathbf{x}$ . This analysis is not feasible through a classical variance- based GSA.

203 Calculation of the indices we propose entails evaluation of conditional moments of  $y(\mathbf{x})$ . This  
 204 step can be computationally very demanding. Along the lines of our discussion about Sobol' indices  
 205 in Sect. 2.1, the new metrics Eq.s (10)-(17) can be evaluated via a surrogate model, as we illustrate  
 206 through our examples in Sect. 3.

### 207 3. Illustrative Examples

208 The theoretical framework introduced in Sect. 2 is here applied to three diverse testbeds: (a)  
 209 the Ishigami function, which constitutes an analytical benchmark typically employed in GSA studies;  
 210 (b) a pumping scenario in a coastal aquifer, where the state variable of interest is the critical pumping  
 211 rate, i.e. the largest admissible pumping rate to ensure that the extraction well is still not contaminated  
 212 by seawater; and (c) a laboratory-scale setting associated with non-reactive transport in porous media.  
 213 In the first two examples the relatively low computational costs associated with the complete  
 214 mathematical description of the target outputs enables us to assess also the error associated with the  
 215 evaluation of indices Eq. (10), Eq. (12), Eq. (14) and Eq. (16) through a gPCE representation of the  
 216 output. In the third case, due to the complexity of the problem and the associated computational costs,  
 217 we relay on the gPCE representation for the target quantity of interest. We emphasize that the use of  
 218 a gPCE as a surrogate model is here considered only as an example, our GSA approach being fully  
 219 compatible with any full model and/or model order reduction technique.



In all of the above scenarios, uncertain parameters  $x_i$  collected in  $\mathbf{x}$  are considered as independent and identically distributed, *i.i.d.*, random variables, each characterized by a uniform distribution within the interval  $\Gamma_i = [x_{i,\min}, x_{i,\max}]$ . All results are grounded on  $5 \times 10^5$  Monte Carlo realizations, enabling convergence of all statistical moments analyzed. Series appearing in the gPCE Eq. (8) are evaluated up to a given order of truncation in all three examples. Here, we apply the total-degree rule and construct a polynomial of order  $w$  through a sparse grid technique (see, e.g., Formaggia et al., 2013 and references therein). We then analyze the way the selected order  $w$  influences the results. Note that the optimal choice of the polynomial  $\psi_p(\mathbf{x})$  in Eq. (8) depends on the pdf of the random variables collected in  $\mathbf{x}$  (Xiu and Karniadakis, 2002). In our exemplary settings we use the multidimensional Legendre polynomials which are orthonormal with respect to the uniform pdf.

### 3.1 Ishigami function

The non-linear and non-monotonic Ishigami function

$$y(\mathbf{x}) = \text{ISH}(\mathbf{x}) = \sin(2\pi x_1 - \pi) + a \sin^2(2\pi x_2 - \pi) + b(2\pi x_3 - \pi)^4 \sin(2\pi x_1 - \pi) \quad (18)$$

is widely used in the literature (e.g., Homma and Saltelli, 1996; Chun et al., 2000; Borgonovo, 2007, 2011; Sudret, 2008; Crestaux et al., 2009) to benchmark GSA methods. Here,  $x_i$  ( $i = 1, 2, 3$ ) are *i.i.d.* random variables uniformly distributed within the interval  $[0, 1]$ . Unconditional mean  $E[\text{ISH}]$ , variance,  $V[\text{ISH}]$ , skewness,  $\gamma[\text{ISH}]$ , and kurtosis,  $k[\text{ISH}]$ , of Eq. (18) can be evaluated analytically as

$$E[\text{ISH}] = \frac{a}{2}, \quad V[\text{ISH}] = \frac{1}{2} + \frac{a^2}{8} + b\pi^4 \left( \frac{1}{5} + \frac{b\pi^4}{18} \right), \quad \gamma[\text{ISH}] = 0, \quad (19a)$$

$$k[\text{ISH}] = \frac{1}{2V^2[\text{ISH}]} \left\{ \frac{3}{4} + b\pi^4 \left[ \frac{3}{5} + b\pi^4 \left( \frac{1}{2} + 3b\pi^4 \left( \frac{1}{13} + \frac{\pi^4 b}{68} \right) \right) \right] + \frac{3}{2} a^2 \left[ \frac{1}{2} + \frac{a^2}{32} + \pi^4 b \left( \frac{1}{5} + \frac{\pi^4 b}{18} \right) \right] \right\}.$$

(19b)



Equation (19) reveals that the unconditional pdf of *ISH* is symmetric with tails that increase with  $|b|$  and decrease with  $|a|$ , as quantified by  $k[ISH]$ . The conditional mean  $E[ISH | x_i]$ , variance  $V[ISH | x_i]$ , skewness  $\gamma[ISH | x_i]$  and kurtosis  $k[ISH | x_i]$  can be evaluated analytically as

$$E[ISH | x_1] = \frac{a}{2} - \frac{1}{5}(5 + b\pi^4)\sin(2\pi x_1), \quad E[ISH | x_2] = a\sin^2(2\pi x_2), \quad E[ISH | x_3] = \frac{a}{2}, \quad (20)$$

$$V[ISH | x_1] = \frac{a^2}{8} + \frac{8b^2\pi^8}{225}(1 - \cos(4\pi x_1)), \quad V[ISH | x_2] = \frac{1}{2} + b\pi^4\left(\frac{1}{5} + \frac{b}{18}\pi^4\right),$$

$$V[ISH | x_3] = \frac{a^2}{8} + \frac{1}{2}\left(1 + b\pi^4(1 - 2x_3)^4\right)^2, \quad (21)$$

$$\gamma[ISH | x_1] = -\frac{128b^3\pi^{12}\sin^3(2\pi x_1)}{4875(V[ISH | x_1])^{3/2}}, \quad \gamma[ISH | x_2] = 0, \quad ISH[y | x_3] = 0, \quad (22)$$

$$k[ISH | x_1] = \frac{1}{V^2[ISH | x_1]} \left\{ \frac{3}{128}a^4 + \frac{4}{75}b^2\pi^8\sin^2(2\pi x_1) \left[ a^2 + \frac{1849}{5525}b^2\pi^8\sin^2(2\pi x_1) \right] \right\},$$

$$k[ISH | x_2] = \frac{1}{2V^2[ISH | x_2]} \left\{ \frac{3}{4} + b\pi^4 \left[ \frac{3}{5} + b\pi^4 \left( \frac{1}{2} + 3b\pi^4 \left( \frac{1}{13} + \frac{1}{68}b\pi^4 \right) \right) \right] \right\}, \quad (23)$$

$$k[ISH | x_3] = \frac{3}{128V^2[ISH | x_3]} \left\{ a^4 + 16 \left( 1 + b\pi^4(1 - 2x_3)^4 \right)^2 \left[ a^2 + \left( 1 + b\pi^4(1 - 2x_3)^4 \right)^2 \right] \right\}.$$

For the sole purpose of illustrating our approach, here and in the following we set  $a = 5$  and  $b = 0.1$ , which corresponds to  $E[ISH] = 2.50$ ,  $V[ISH] = 10.84$  and  $k[ISH] = 4.18$ . Figure 1 depicts the first four moments of *ISH* conditional to values of  $x_1$  (blue curves),  $x_2$  (red curves) and  $x_3$  (green curves) within the parameter space. The corresponding unconditional moments (black curves) are also depicted for completeness.

Comparing Eq. (19a) and Eq. (20), it is seen that  $E[ISH | x_3]$  coincides with its unconditional counterpart  $E[ISH]$ , indicating that conditioning on any value of  $x_3$  does not impact the mean of *ISH*. Otherwise, setting  $x_1$  or  $x_2$  to a given value clearly affects the mean of *ISH* in a way which is governed by Eq. (20) and shown in Fig. 1a. It is clear from Eq. (20) that  $E[ISH | x_2]$  has a higher



frequency of oscillation within  $\Gamma_{x_2}$  than has  $E[ISH | x_1]$  within  $\Gamma_{x_1}$ . The global index in Eq. (10)

can be evaluated analytically as

$$AMAE_{x_1} = \frac{4}{a\pi} \left| 1 + \frac{b}{5} \pi^4 \right|, \quad AMAE_{x_2} = \frac{2}{\pi} \frac{|a|}{a}, \quad AMAE_{x_3} = 0. \quad (24)$$

Note that  $AMAE_{x_2}$  does not depend on specific values of  $a$  and  $b$ .

Equation (21) shows that all random model parameters influence the variance of  $ISH$ , albeit to different extents, as also illustrated in Fig. 1b. Note that  $V[ISH | x_2]$  is always smaller than  $V[ISH]$  (compare Eq. (19a) and Eq. (21)) and does not depend on  $x_2$ , i.e., conditioning  $ISH$  on  $x_2$  reduces the process variance regardless the conditioning value. Otherwise,  $V[ISH | x_3]$  can be significantly larger or smaller than its unconditional counterpart. Table 1 lists values of  $AMAV_{x_i}$  ( $x_i = x_1, x_2, x_3$ ) computed via Eq. (12) with the  $a$  and  $b$  values selected for our demonstration. The principal Sobol' indices (Sudret, 2008)

$$S_{x_1} = \frac{(5 + b\pi^4)^2}{50 V[ISH]}, \quad S_{x_2} = \frac{a^2}{8 V[ISH]}, \quad S_{x_3} = 0, \quad (25)$$

are also listed for completeness. As expected, values of  $AMAV_{x_i}$  listed in Table 1 suggest that conditioning on  $x_3$  has the strongest impact on the variance of  $ISH$ , followed by  $x_1$  and  $x_2$ . Note that  $S_{x_3} = 0$ , a result which might be interpreted as a symptom that  $ISH$  is insensitive to  $x_3$ . The apparent inconsistency between the conclusions which could be drawn by analysing  $AMAV_{x_3}$  and  $S_{x_3}$  is reconciled by the observation that the function  $V[ISH] - V[ISH | x_3]$  can be positive and negative in a way that its integration over  $\Gamma_{x_3}$  vanishes (see also Fig. 1b). Therefore, the mean reduction of the variance of  $ISH$  due to knowledge of (or conditioning on)  $x_3$  is zero. It is remarked that this



277 observation does not imply that the variance of *ISH* does not vary with  $x_3$ , as clearly highlighted by  
 278 Fig. 1b and quantified by  $AMAV_{x_3}$ .

279 The symmetry of the pdf of *ISH* is not affected by conditioning on  $x_2$  or  $x_3$ , as demonstrated  
 280 by Eq. (22). Otherwise,  $\gamma[ISH | x_1]$  is left (or right) skewed when  $x_1$  is smaller (or larger) than 0.5,  
 281 as dictated by Eq. (22) and shown in Fig. 1c.

282 The conditional kurtosis  $k[ISH | x_2]$  does not depend on the conditioning value  $x_2$  (see Eq.  
 283 (23)). We then note that this conditional moment is always larger than (or equal to) its unconditional  
 284 counterpart  $k[ISH]$ , regardless the particular values assigned to  $a$  and  $b$ , as we verified through  
 285 extensive numerical tests. This result implies that the pdf of *ISH* conditional on  $x_2$  is characterized  
 286 by tails which are heavier than those of its unconditional counterpart. Figure 1d reveals that  
 287  $k[ISH | x_1]$  and  $k[ISH | x_3]$  are smaller than  $k[ISH]$  for the values of  $a$  and  $b$  implemented in this  
 288 example. Table 1 lists the resulting values of  $AMAk_{x_i}$  ( $x_i = x_1, x_2, x_3$ ) for the selected  $a$  and  $b$   
 289 values.

290 We close this part of the study by investigating the error which would arise when one evaluates  
 291 our GSA indices by replacing *ISH* through a gPCE surrogate model. We do so on the basis of the  
 292 absolute relative error

$$293 \quad e_j = \begin{cases} \left| \frac{j_{gPCE} - j_{full\ model}}{j_{full\ model}} \right| & \text{if } j_{full\ model} \neq 0 \\ \left| j_{gPCE} - j_{full\ model} \right| & \text{if } j_{full\ model} = 0 \end{cases}, \quad (26)$$

294 where  $j = AMAE_{x_i}, AMAV_{x_i}, AMA\gamma_{x_i}$  or  $AMAk_{x_i}$  ( $x_i = x_1, x_2, x_3$ ); the subscripts *full model* and  
 295 *gPCE* respectively indicate that quantity  $j$  is evaluated via Eq. (18) or through a gPCE surrogate  
 296 model, constructed as outlined in Sect. 2.1. Figure 2 depicts Eq. (26) versus the total degree  $w$  of the  
 297 gPCE. Note that the lower limit of the vertical axis of Fig. 2 is set to 0.001% for convenience of  
 298 graphical representation. Approximation errors associated with GSA indices related to the mean,



299  $AMAE_{x_i}$ , rapidly approach zero as  $w$  increases. Note that  $e_{AMAE_{x_3}}$  is smaller than 0.001% for all tested  
 300 values of  $w$  and it is therefore not included in Fig. 2a. Values of  $e_j$  linked to  $AMAV_{x_i}$ ,  $AMAY_{x_i}$  and  
 301  $AMAK_{x_i}$  do not show a consistently decreasing trend until  $w \geq 5$ . Values of  $e_j$  associated with the  
 302 variance, skewness and kurtosis decrease with approximately the same average linear rate (in log-log  
 303 scale) for the largest  $w$  considered (Figs 2b, 2c and 2d). This example reinforces the need for reliably  
 304 testing the accuracy of a gPCE-based model approximation as a function of the total degree desired,  
 305 depending on the statistical moment of interest.

### 3.2 Critical Pumping Rate in Coastal Aquifers

306  
 307 The example we consider here is taken from the study of Pool and Carrera (2011) related to  
 308 the analysis of salt water contamination of a pumping well operating in a homogenous confined  
 309 coastal aquifer of uniform thickness  $b'$ . The setting is sketched in Fig. 3. A constant discharge,  $Q_w'$   
 310 [ $L^3 T^{-1}$ ], is pumped from a fully penetrating well located at a distance  $x_w'$  [L] from the coastline and  
 311 a constant freshwater flux,  $q_f'$  [ $L T^{-1}$ ], flowing from the inland to the coastline, is set. Pool and Carrera  
 312 (2011) introduced a dimensionless well discharge  $Q_w = Q_w' / (b' x_w' q_f')$  and defined the critical  
 313 pumping rate  $Q_c$  as the value of  $Q_w$  at which a normalized solute concentration monitored at the well  
 314 exceeds 0.1%. A key result of the study of Pool and Carrera (2011) is that  $Q_c$  can be approximated  
 315 through the following implicit equation

$$316 \quad \lambda_D = 2 \left[ 1 - \frac{Q_c}{\pi} \right]^{1/2} + \frac{Q_c}{\pi} \ln \frac{1 - (1 - Q_c / \pi)^{1/2}}{1 + (1 - Q_c / \pi)^{1/2}} \quad \text{with} \quad \lambda_D = \frac{\Delta \rho'}{\rho_f'} \frac{1 - (Pe_T)^{-1/6}}{x_w' J} \quad (27)$$

317 Here,  $x_w = x_w' / b'$ ;  $J = q_f' / K$ ;  $Pe_T = b' / \alpha_T'$ ;  $K$  [ $L T^{-1}$ ] is the uniform hydraulic conductivity;  $\alpha_T'$  [L]  
 318 is transverse dispersivity;  $\Delta \rho' = \rho_s' - \rho_f'$ ,  $\rho_f'$  and  $\rho_s'$  being fresh- and salt-water densities,  
 319 respectively. The quantity  $Pe_T$  is a measure of the intensity of dispersive effects,  $J$  is the natural head  
 320 gradient of the incoming freshwater, and  $x_w$  is the dimensionless distance of the well from the





coastline. Pool and Carrera (2011) demonstrated the accuracy of Eq. (27) in predicting the critical pumping rate when  $\lambda_d \in (0-10]$ . Additional details about the problem setting, boundary and initial conditions, as well as geometrical configuration of the system can be found in Pool and Carrera (2011). Here, we focus on the main result of Eq. (27) which represents the complete mathematical description of the problem we analyze. We perform a sensitivity analysis of  $Q_c$  with respect to  $Pe_T$ ,  $J$ , and  $x_w$ . While the first two quantities are difficult to characterize experimentally in practical applications, the well location can be considered as an operational/design variable. Table 2 lists the intervals of variation we consider for  $Pe_T$ ,  $J$  and  $x_w$ . These are designed to (a) resemble realistic field values and (b) obey the above mentioned constraint about  $\lambda_d$ .

Numerical evaluation of the first four unconditional statistical moment of  $Q_c$  yields a mean value  $E[Q_c] = 1.65$ , variance  $V[Q_c] = 0.17$ , skewness  $\gamma[Q_c] = -0.30$  (which indicates a light asymmetry in the pdf), and kurtosis  $k[Q_c] = 2.51$  (i.e., pdf tails decrease faster than those of a Gaussian distribution). Figure 4 depicts the first four moments of  $Q_c$  conditional to values of  $Pe_T$  (blue curves),  $J$  (green curves), and  $x_w$  (red curves) within the parameter space. The corresponding unconditional moments (black curves) are also depicted for completeness. Note that each parameter interval of variation has been normalized to span the range  $[0, 1]$  for graphical representation purposes. Table 3 lists the values of indices  $AMAE_{x_i}$ ,  $AMAV_{x_i}$ ,  $S_{x_i}$ ,  $AMA\gamma_{x_i}$  and  $AMAk_{x_i}$  ( $x_i = Pe_T, J, x_w$ ) associated with  $Q_c$ . As in our first example, it is clear that sensitivity of  $Q_c$  with respect to  $Pe_T, J, x_w$  depends on the statistical moment of interest.

Inspection of Fig. 4a reveals that the mean of  $Q_c$  is more sensitive to conditioning on  $J$  or  $x_w$  than to conditioning on  $Pe_T$ . Note that increasing  $Pe_T$ , i.e., considering advection-dominated scenarios, leads to an increase of the mean value of  $Q_c$ . This is so because the dispersion of the intruding saltwater wedge is diminished and the travel time of solutes to the well tends to increase.



High values of the natural head gradient of the incoming freshwater,  $J$ , are associated with high mean values of  $Q_c$ . This is consistent with the observation that the inland penetration of the wedge is contrasted by the effect of freshwater which flows in the opposite direction. As expected, decreasing  $x_w$  (moving the pumping well towards the coast) leads to a reduction of the mean value of  $Q_c$ . Figure 4a shows that mean  $Q_c$  varies with  $x_w$  and  $J$  in a similar way. This outcome is consistent with Eq. (27) where  $Q_c$  depends on the product  $x_w J$ , i.e., increasing  $x_w$  or  $J$  has the same effect on  $Q_c$ .

It can be noted (see Tab. 3) that  $AMAE_{Pe_T}$  is smaller than  $AMAE_J$  and  $AMAE_{x_w}$ , consistent with Fig. 4a. Figure 4b shows that the variance of  $Q_c$  decreases as  $Pe_T$ ,  $J$ , or  $x_w$  increase. This trend suggests that the uncertainty on  $Q_c$ , as quantified by the variance, decreases as (i) the intruding wedge sharpens or is pushed toward the seaside boundary by the incoming freshwater or (ii) the well is placed at increasing distance from the coastline. Inspection of Fig. 4c and 4d shows that conditioning on  $Pe_T$ ,  $J$ , or  $x_w$  causes the pdf of  $Q_c$  to become less asymmetric and less tailed than its unconditional counterpart. This behavior suggests that the relative frequency of occurrence of (high or low) extreme values of  $Q_c$  tends to decrease as additional information about the model parameters become available.

Figure 5 depicts error,  $e_j$ , Eq. (26) versus total degree,  $w$ , of the gPCE representation of  $Q_c$ , for  $j =$  (a)  $AMAE_{x_i}$ , (b)  $AMAV_{x_i}$ , (c)  $AMAY_{x_i}$  and (d)  $AMAK_{x_i}$  ( $x_i = Pe_T$  (blue curves),  $J$  (red curves),  $x_w$  (green curves)). These results indicate that: (i)  $e_j$  associated with  $AMAE_{x_i}$  is negligible ( $\approx 1\%$ ) even for low  $w$ ; (ii)  $e_{AMAV_{Pe_T}} \approx 10\%$  for  $w = 2$  and rapidly decreases to values below 1% for increasing  $w$ ; (iii)  $e_{AMAV_J}$  and  $e_{AMAV_{x_w}}$  are always smaller than 1%; and (iv) the trend of  $e_{AMAY_{x_i}}$  is similar to that of  $e_{AMAK_{x_i}}$  for all  $x_i$ , with values of the order of 10% or higher for  $w = 2$  and displaying a decrease with increasing  $w$  to then stabilize around values smaller than 1% when  $w \approx 4$  or 5. It is then clear from Fig. 5 that attaining a given acceptable level of accuracy for the gPCE-based



approximation of our moment-based GSA indices for  $Q_c$  requires increasing the total order  $w$  of the gPCE with the order of the statistical moment considered. As such, following the typical practice of assessing the reliability of a gPCE surrogate model solely on the basis of the variance or of a few random model realizations does not guarantee a satisfactory accuracy of the uncertainty analysis of a target model output which should consider higher-order statistical moments.

### 3.3 Solute transport in a laboratory-scale porous medium with zoned heterogeneity

As a last exemplary showcase, we consider the laboratory-scale experimental analysis of nonreactive chemical transport illustrated by Esfandiar et al. (2015). These authors consider tracer transport within a rectangular flow cell filled with two types of uniform sands. These were characterized by diverse porosity and permeability values, which were measured through separate, standard laboratory tests. A sketch of the experimental set-up displaying the geometry of the two uniform zones respectively formed by coarse and fine sand is illustrated in Fig. 6.

After establishing fully saturated steady-state flow, a solution containing a constant tracer concentration is injected as a step input at the cell inlet. The tracer breakthrough curve is then defined in terms of the temporal variation of the spatial mean of the concentration detected along the flow cell outlet. Esfandiar et al. (2015) modeled the temporal evolution of normalized (with respect to the solute concentration of the injected fluid) concentration at the outlet,  $\bar{C}(t)$  ( $t$  denoting time), by numerically solving within the flow domain the classical Advection-Dispersion Equation implementing an original and accurate space-time grid adaptation technique. Unknown longitudinal dispersivities of the two sands ( $a_{L,i}$ ,  $i = 1, 2$  respectively denoting the coarse and fine sand) were considered as uncertain system parameters to be estimated against the available experimental solute breakthrough data. To minimize the computational costs in the model calibration process, Esfandiar et al. (2015) relied on a gPCE approximation of  $\bar{C}(t)$ . The authors constructed a gPCE of total degree  $w = 3$  by considering  $\log_{10}(a_{L,i})$  to be two *i.i.d.* random variables uniformly distributed within



391  $\Gamma_{\log_{10}(a_{L,i})} = [-6, -2]$ ,  $a_{L,i}$  being expressed in [m]. Further details about the problem set-up, numerical  
 392 discretization and grid adaptation technique as well of the construction of the gPCE representation  
 393 can be found in Esfandiar et al. (2015). Here, we ground the application of our new GSA metrics on  
 394 the gPCE surrogate model already constructed by Esfandiar et al. (2015) to approximate  $\bar{C}(t)$ .

395 Figure 7 depicts the temporal evolution of the unconditional expected value,  $E[\bar{C}(t)]$ ,  
 396 variance,  $V[\bar{C}(t)]$ , skewness,  $\gamma[\bar{C}(t)]$ , and kurtosis,  $k[\bar{C}(t)]$ , of normalized  $\bar{C}(t)$ . Time steps  
 397  $t_{0.02}$ ,  $t_{0.4}$ , and  $t_{0.96}$ , i.e., the times at which  $E[\bar{C}(t)] = 0.02, 0.4$ , and  $0.96$ , respectively, are  
 398 highlighted in Fig. 7a. Figure 7a reveals a pronounced tailing of  $E[\bar{C}(t)]$  at late times, the short  
 399 time mean breakthrough being associated with a rapid temporal increase of  $E[\bar{C}(t)]$ . A local  
 400 minimum at  $t_{0.4}$  and two local peaks are recognized in  $V[\bar{C}(t)]$  (Fig. 7b). The variance peaks  
 401 at times approximately corresponding to the largest values of  $\partial^2 E[\bar{C}(t)] / \partial t^2$ . This outcome is  
 402 consistent with the results of numerical Monte Carlo (MC) simulations depicted in Fig. 8 of Esfandiar  
 403 et al. (2015) where the largest spread of the MC results is observed around these locations. The local  
 404 minimum displayed by  $V[\bar{C}(t)]$  suggests that  $\bar{C}(t)$  at observation times close to  $t_{0.4}$  is mainly  
 405 driven by advection, consistent with the observation that advective transport components are the main  
 406 driver of the displacement of the center of mass of a solute plume. The late time variance  $V[\bar{C}(t)]$   
 407 tends to vanish because the normalized breakthrough curve is always very close to unity irrespective  
 408 of the values of  $a_{L,1}$  and  $a_{L,2}$ . Joint inspection of Figs 7c and 7d reveals that the pdf of  $\bar{C}(t)$  tends to  
 409 be symmetric around the mean (Fig. 7c) and characterized by light tails (Fig. 7d) at about  $t_{0.4}$ .  
 410 Otherwise, the pdfs of  $\bar{C}(t)$  tends to display heavy right or left tails, respectively for observation  
 411 times shorter or longer than  $t_{0.4}$ . These observations suggest that the relative frequency of rare events



(i.e., very low or high solute concentrations, which can be of some concern in the context of risk assessment) is lowest at intermediate observation times across the duration of the experiment.

Figure 8 depicts the temporal evolution of (a)  $AMAE_{x_i}$ , (b)  $AMAV_{x_i}$ , (c)  $AMAY_{x_i}$ , and (d)  $AMAK_{x_i}$  ( $x_i = \log_{10}(a_{L,1}), \log_{10}(a_{L,2})$ ) of  $\bar{C}(t)$ . Results embedded in Fig. 8 show that statistical moments of  $\bar{C}(t)$  are more sensitive to  $\log_{10}(a_{L,1})$  than to  $\log_{10}(a_{L,2})$  at early times. The opposite occurs when  $t > t_{0.4}$ . Our set of results suggests that the overall early time pattern of solute breakthrough is mainly dictated by the value of  $a_{L,1}$ , the late time behavior being chiefly influenced by  $a_{L,2}$ . These conclusions are supported by the results of Figs 9-11, where we depict the expected value, variance, skewness, and kurtosis of  $\bar{C}(t)$  conditional to  $\log_{10}(a_{L,1})$  (blue curves) and  $\log_{10}(a_{L,2})$  (red curves), at times  $t = t_{0.02}$  (Fig. 9),  $t_{0.4}$  (Fig. 10), and  $t_{0.96}$  (Fig. 11). The corresponding unconditional moments are also depicted (black curves) for ease of comparison. Figure 9 shows that the first four statistical moments of  $\bar{C}(t_{0.02})$  are practically insensitive to the value of the fine sand dispersivity,  $a_{L,2}$ . As one could expect by considering the relative size and geometrical pattern of the two sand zones, Fig. 9a shows that the average amount of solute reaching the cell outlet at early times increases with  $a_{L,1}$ , because dispersion of solute increases through the coarse sand which resides in the largest portion of the domain. Figure 9b shows  $V[\bar{C}(t_{0.02})]$  is negligible when  $a_{L,1}$  is known. Consistent with this result, Figs 9c and 9d respectively show a reduction in the asymmetry and in the tailing behavior of the pdf of  $\bar{C}(t_{0.02})$  when  $a_{L,1}$  is fixed. These results are a symptom of a reduced process uncertainty, which is in line with the observation that the bulk of the domain is filled with the coarse sand whose dispersive properties become deterministic when  $a_{L,1}$  is known.

Inspection of the first four unconditional statistical moments of  $\bar{C}(t_{0.4})$  (black curves in Fig. 10) indicates that the unconditional pdf of  $\bar{C}$  at this intermediate time is closely resembling a



434 Gaussian distribution. Conditioning  $\bar{C}(t_{0.4})$  on dispersivity causes a variance reduction, an increase  
 435 of the tailing and the appearance of a negative (left) or positive (right) skewness, respectively when  
 436 conditioning is performed on  $a_{L,1}$  or  $a_{L,2}$ . The latter behavior suggests that in the type of experimental  
 437 setting analyzed the variability of  $a_{L,1}$  promotes the appearance of values of  $\bar{C}(t_{0.4})$  larger than the  
 438 mean, the opposite occurring when solely  $a_{L,2}$  is considered as uncertain.

439 Figure 11 shows that all four statistical moment of  $\bar{C}(t_{0.96})$  are chiefly sensitive to the  
 440 dispersivity of the fine sand box, which is placed near the cell outlet. One can note that knowledge of  
 441  $a_{L,2}$  yields a diminished variance of  $\bar{C}(t_{0.96})$ , which drops almost to zero, an increased degree of  
 442 symmetry and a reduce tailing of the pdf of  $\bar{C}(t_{0.96})$ , all these evidences being symptoms of  
 443 uncertainty reduction.

444 Results depicted in Figs 9-11 and our earlier observations about Fig. 7 are consistent with the  
 445 expected behavior of transport in the system and the relative role of the dispersivities of the two sand  
 446 regions. The high level of sensitivity of  $\bar{C}(t)$  to  $a_{L,1}$  at the early times of solute breakthrough is in  
 447 line with the observation that solute particles are mainly advected and dispersed through the coarse  
 448 sand. Both dispersivities affect the behavior of  $\bar{C}(t)$  at intermediate times, when solute is traveling  
 449 through both sands. The dispersivity of the coarse sand plays a minor role at late times, because  
 450 virtually no concentration gradients arise in this portion of the domain. Otherwise, concentration  
 451 gradients persist in the fine sand zone close to the outlet and the solute breakthrough is clearly  
 452 controlled by the dispersive properties of the fine sand.

#### 453 **4. Conclusions**

454 We introduce a set of new indices to be employed in the context of global sensitivity analysis,  
 455 GSA, of hydrological and Earth systems. These indices consider the first four (statistical) moments  
 456 of the probability density function, pdf, of a desired model output,  $y$ . As such, they quantify the



457 expected relative variation, due to the variability in one (or more) model input parameter(s) of the  
458 expected value, variance, skewness and kurtosis of  $y$ . When viewed in the current research trend, our  
459 work is intended to bridge the gap between variance-based and pdf-based GSA approaches since it  
460 embeds the simplicity of the former while allowing for a higher-order description of how the structure  
461 of the pdf of  $y$  is affected by variations of uncertain model parameters. We cope with computational  
462 costs, which might be high when evaluating higher-order moments, by coupling our GSA approach  
463 with techniques approximating the full model response through a surrogate model. For the sake of  
464 our study, we consider the generalized Polynomial Chaos Expansion (gPCE), other model reduction  
465 techniques being fully compatible with our approach. Our new indices can be of interest in  
466 applications in the context of current practices and evolution trends in factor fixing procedures (i.e.,  
467 assessment of the possibility of fixing a parameter value on the basis of the associated output  
468 sensitivity), design of experiment, uncertainty quantification and environmental risk assessment, due  
469 to the role of the key features of a model output pdf in such analyses.

470 We test and exemplify our methodology on three testbeds: (a) the Ishigami function, which is  
471 widely employed to test sensitivity analysis techniques, (b) the evaluation of the critical pumping rate  
472 to avoid salinization of a pumping well in a coastal aquifer, and (c) a laboratory-scale nonreactive  
473 transport experiment. Our theoretical analyses and application examples lead to the following major  
474 conclusions.

- 475 1. The sensitivity of a model output,  $y$ , with respect to a parameter depends on the selected global  
476 sensitivity index, i.e., variability of a model parameter affects statistical moments of  $y$  in different  
477 ways and with different relative importance, depending on the statistical moment considered.  
478 Relying on the indices we propose allows enhancing our ability to quantify how model parameters  
479 affect features of the model output pdf, such as mean, degree of spread, symmetry and tailedness,  
480 in a straightforward and easily transferrable way.
- 481 2. Joint inspection of our moment-based global sensitivity indices and of the first four statistical  
482 conditional and unconditional moments of  $y$  increases our ability to understand the way the



483 structure of the model output pdf is controlled by model parameters. As demonstrated in our  
484 examples, classical variance-based GSA methods cannot be used for this purpose, leading, in  
485 some cases, to the unwarranted conclusion that a given parameter have a limited impact on a  
486 target output.

487 3. Analysis of the errors associated with the use of a surrogate model for the evaluation of our  
488 moment-based sensitivity indices suggests that the construction of a surrogate model with  
489 increasing level of accuracy (as rendered, in our examples, by the total degree  $w$  of gPCE  
490 approximation) might be required, depending on the statistical moment considered in the GSA,  
491 i.e., depending on the target statistical moment of  $y$ .

492





## 493 References

- 494 Borgonovo, E.: A new uncertainty importance measure, *Reliability Eng. Syst. Safety*, 92, 771-784,  
495 2007.
- 496 Borgonovo, E., Castaings, W., and Tarantola, S.: Moment Independent Importance Measures: New  
497 Results and Analytical Test Cases, *Risk Anal.*, 31, 404-428, 2011.
- 498 Chu, J., Zhang, C., Fu, G., Li, Y. and Zhou, H.: Improving multi-objective reservoir operation  
499 optimization with sensitivity-informed dimension reduction, *Hydrol. Earth Syst. Sci.*, 19, 3557-3570,  
500 doi:10.5194/hess-19-3557-2015, 2015.
- 501 Chun, M. H., Han, S. J. and Tak, N. I. L.: An uncertainty importance measure using a distance metric  
502 for the change in a cumulative distribution function, *Reliab. Eng. Syst. Saf.*, 70, 313-321, 2000.
- 503 Ciriello, V., Di Federico, V., Riva, M., Cadini, F., De Sanctis, J., Zio, E. and Guadagnini, A.:  
504 Polynomial chaos expansion for global sensitivity analysis applied to a model  
505 of radionuclide migration in a randomly heterogeneous aquifer, *Stoch. Environ. Res. Risk. Assess.*,  
506 27, 945-954, <http://dx.doi.org/10.1007/s00477-012-0616-7>, 2013.
- 507 Colombo, I., Porta, G.M., Ruffo, P. and Guadagnini, A.: Uncertainty quantification of overpressure  
508 buildup through inverse modeling of compaction processes in sedimentary basins, *Hydrogeol. J.*,  
509 doi:10.1007/s10040-016-1493-9, 2016.
- 510 Crestaux, T., Le Maître, O. and Martinez, J. M.: Polynomial chaos expansion for sensitivity analysis,  
511 *Reliab. Eng. Syst. Safety*, 94(7), 1161-1172, <http://dx.doi.org/10.1016/j.ress.2008.10.008>, 2009.
- 512 Elshorbagy, A., Corzo, G., Srinivasulu, S., and Solomatine, D. P.: Experimental investigation of the  
513 predictive capabilities of data driven modeling techniques in hydrology - Part 1: Concepts and  
514 methodology, *Hydrol. Earth Syst. Sci.*, 14, 1931-1941, doi:10.5194/hess-14-1-2010, 2010a.
- 515 Elshorbagy, A., Corzo, G., Srinivasulu, S. and Solomatine, D. P.: Experimental investigation of the  
516 predictive capabilities of data driven modeling techniques in hydrology - Part 2: Application, *Hydrol.*  
517 *Earth Syst. Sci.*, 14, 1943-1961, doi:10.5194/hess-14-1943-2010, 2010b.
- 518 Esfandiar, B., Porta, G., Perotto, S. and Guadagnini, A.: Impact of space-time mesh adaptation on  
519 solute transport modeling in porous media, *Water Resour. Res.*, 51, 1315-1332,  
520 doi:10.1002/2014WR016569, 2015.
- 521 Formaggia, L., Guadagnini, A., Imperiali, I., Lever, V., Porta, G., Riva, M., Scotti, A. and Tamellini,  
522 L.: Global sensitivity analysis through polynomial chaos expansion of a basin-scale geochemical  
523 compaction model, *Comput. Geosci.*, 17, 25-42, <http://dx.doi.org/10.1007/s10596-012-9311-5>, 2013.
- 524 Förster, K., Meon, G., Marke, T. and Strasser, U.: Effect of meteorological forcing and snow model  
525 complexity on hydrological simulations in the Sieber catchment (Harz Mountains, Germany), *Hydrol.*  
526 *Earth Syst. Sci.*, 18, 4703-4720, doi:10.5194/hess-18-4703-2014, 2014.
- 527 Fu, G., Kapelan, Z. and Reed, P.: Reducing the complexity of multiobjective water distribution  
528 system optimization through global sensitivity analysis, *J. Water Resour. Plann. Manage.*, 38(3), 196-  
529 207, doi:0.1061/(ASCE)WR.1943-5452.0000171, 2012.
- 530 Ghanem, R. G and Spanos, P. D.: *Stochastic finite elements: a spectral approach*, Berlin: Springer;  
531 1991.



- 532 Gläser, D., Dell'Oca, A., Tatomir, A., Bensabat, J., Class, H., Guadagnini, A., Helmig, R.,  
533 McDermott, C., Riva, M., and Sauter, M.: An approach towards a FEP-based model risk assessment  
534 for hydraulic fracturing operations, *Energ. Procedia*, 97, 387-394, 2016.
- 535 Grauso, G., Fattoruso, G., Crocetti C. and Montanari, A.: A spatially distributed analysis of erosion  
536 susceptibility and sediment yield in a river basin by means of geomorphic parameters and regression  
537 relationships, *Hydrol. Earth Syst. Sci. Discussions*, 4, 627-654, 2007.
- 538 Hartmann, A., Weiler, M., Wagener, T., Lange, J., Kralik, M., Humer, F., Mizyed, N., Rimmer, A.,  
539 Barbera, J. A., Andreo, B., Butscher, C. and Huggenberger, P.: Process-based karst modelling to  
540 relate hydrodynamic and hydrochemical characteristics to system properties, *Hydrol. Earth Syst. Sci.*,  
541 17, 3305-3321, doi:10.5194/hess-17-3305-2013, 2013.
- 542 Herman, J. D., Kollat, J. B., Reed, P. M. and Wagener, T.: From maps to movies: high-resolution  
543 time-varying sensitivity analysis for spatially distributed watershed models, *Hydrol. Earth Syst. Sci.*,  
544 17, 5109-5125, doi:10.5194/hess-17-5109-2013, 2013.
- 545 Homma, T. and Saltelli, A.: Importance measures in global sensitivity analysis of nonlinear models,  
546 *Reliab. Eng. Syst. Saf.*, 52, 1-17, 1996.
- 547 Iman, R.L. and Hora, S. C.: A robust measure of uncertainty importance for use in fault tree system  
548 analysis, *Risk Anal.*, 10(3), 401-406, 1990.
- 549 Koutsoyiannis, D.: "A random walk on water", *Hydrol. Earth Syst. Sci.*, 14, 585-601, 2010.
- 550 Krykacz-Hausmann, B.: Epistemic sensitivity analysis based on the concept of entropy, In: Prado, P.,  
551 Bolado, R. (Eds.), *Proceedings of SAMO2001*, Madrid, pp. 31-35, 2001.
- 552 Le Maître, O. P. and Knio, O. M.: *Spectral methods for uncertainty quantification*, Scientific  
553 computation, Springer, 2010.
- 554 Paniconi, C. and Putti, M.: Physically based modeling in catchment hydrology at 50: survey and  
555 outlook, *Water Resour. Res.*, 51, 7090-7129, doi:10.1002/2015WR017780, 2015.
- 556 Pianosi, F. and Wagener, T.: A simple and efficient method for global sensitivity analysis based on  
557 cumulative distribution functions, *Environ. Model. Softw.*, 67, 1-11,  
558 <http://dx.doi.org/10.1016/j.envsoft.2015.01.004>, 2015.
- 559 Pianosi, F., Wagener, T., Beven, K., Freer, J., Hall, J.W., Rougier, J. and Stephenson, D.B.:  
560 Sensitivity Analysis of Environmental Models: a Systematic Review with Practical Workflow,  
561 *Environmental Modelling & Software*, 79, 214-232, <http://dx.doi.org/10.1016/j.envsoft.2016.02.008>,  
562 2016.
- 563 Pool, M. and Carrera, J.: A correction factor to account for mixing in Ghyben-Herzberg and critical  
564 pumping rate approximations of seawater intrusion in coastal aquifers, *Water Resour. Res.*, 47,  
565 W05506, doi:10.1029/2010WR010256, 2011.
- 566 Punzo, V., Marcello, M. and Biagio, C.: Do we really need to calibrate all the parameters? Variance-  
567 based sensitivity analysis to simplify microscopic traffic flow models, *Intel. Trans. Sys. IEEE Trans.*,  
568 16(1), 184-193, 2015.
- 569 Razavi, S. and Gupta H. V.: What do we mean by sensitivity analysis? The need for comprehensive  
570 characterization of "global" sensitivity in Earth and Environmental systems models, *Water Resour.*  
571 *Res.*, 51, doi:10.1002/2014WR016527, 2015.



- 572 Razavi, S., Tolson, B.A. and Burn, D.H.: Numerical assessment of metamodelling strategies in  
573 computationally intensive optimization, *Environ. Model. Softw.*, 34(0), 67-86,  
574 <http://dx.doi.org/10.1016/j.envsoft.2011.09.010>, 2012a.
- 575 Razavi, S., Tolson, B.A. and Burn, D.H.: Review of surrogate modeling in water resources. *Water*  
576 *Resour. Res.* 48 (7), W07401, <http://dx.doi.org/10.1029/2011WR011527>, 2012b.
- 577 Riva, M., Guadagnini, A. and Dell'Oca, A.: Probabilistic assessment of seawater intrusion under  
578 multiple sources of uncertainty, *Adv. Water Resour.*, 75, 93-104,  
579 <http://dx.doi.org/10.1016/j.advwatres.2014.11.002>, 2015.
- 580 Saltelli, A., Ratto, M., Andres, T., Campolongo, F., Cariboni, J., Gatelli, D., Saisana, M., Tarantola,  
581 S.: *Global Sensitivity Analysis. The Primer*. Wiley, 2008.
- 582 Sarrazin, F., Pianosi, F. and Wagener, T.: Global sensitivity analysis of environmental models:  
583 convergence and validation, *Environ. Model. Softw.*, 79, 135-152,  
584 <http://dx.doi.org/10.1016/j.envsoft.2016.02.005>, 2016.
- 585 Sobol, I. M.: Sensitivity estimates for nonlinear mathematical models, *Math. Model. Comput. Exp.*,  
586 1, 407-417, 1993.
- 587 Sudret, B.: Global sensitivity analysis using polynomial chaos expansions, *Reliab. Eng. & Syst.*  
588 *Safety*, 93, 964-979, doi:10.1016/j.ress.2007.04.002, 2008.
- 589 Wagener, T. and Montanari, A.: Convergence of approaches toward reducing uncertainty in  
590 predictions in ungauged basins, *Water Resour. Res.*, 47, W060301, doi:10.1029/2010WR009469,  
591 2011.
- 592 Wagener, T., Sivapalan, M., Troch, P. A., McGlynn, B. L., Harman, C. J., Gupta, H. V., Kumar, P.,  
593 Rao, P. S. C., Basu, N. B., and Wilson, J. S.: The future of hydrology: An evolving science for a  
594 changing world, *Water Resour. Res.*, 46, W05301, doi:10.1029/2009WR008906, 2010.
- 595 Willmann, M., Sanchez-Vila, X., Carrera, J. and Guadagnini, A.: Block-upscaling of transport in  
596 heterogeneous aquifers, *Calibration and Reliability in Groundwater Modelling: From Uncertainty to*  
597 *Decision Making*, *Proceedings of ModelCARE 2005*, The Hague, The Netherlands, June 2005, IAHS  
598 Publ. 304, 2006.
- 599 Xiu, D. and Karniadakis, G. E. M.: The Wiener-Askey polynomial chaos for stochastic differential  
600 equations, *SIAM J. Sci. Comput.*, 24(2), 619-644, <http://dx.doi.org/10.1137/S1064827501387826>,  
601 2002.
- 602



603

604 **Table 1.** Global sensitivity index  $AMAE_{x_i}$  Eq. (10),  $AMAV_{x_i}$  Eq. (12),  $AMAY_{x_i}$  Eq. (14), and  
 605  $AMAK_{x_i}$  Eq. (16) associated with the Ishigami function Eq. (18). Principal Sobol' indices,  $S_{x_i}$  Eq.  
 606 (7), are also listed;  $x_i = x_1, x_2, x_3$ .

	$AMAE_{x_i}$	$AMAV_{x_i}$	$S_{x_i}$	$AMAY_{x_i}$	$AMAK_{x_i}$
$x_1$	0.75	0.40	0.40	0.45	0.37
$x_2$	0.64	0.29	0.29	0.00	0.33
$x_3$	0.00	0.84	0.00	0.00	0.53

607

608



609 **Table 2.** Intervals of variations of  $Pe_T$ ,  $J$ ,  $x_w$ .

	$\Gamma_n = [x_{n,\min} - x_{n,\max}]$
$\Gamma_{Pe_T}$	[0.01 – 0.1]
$\Gamma_J$	$[8e^{-4} - 2.5e^{-3}]$
$\Gamma_{x_w}$	[10 – 33]

610

611



612 **Table 3.** Global sensitivity index  $AMAE_{x_i}$  Eq. (10),  $AMAV_{x_i}$  Eq. (12),  $AMAY_{x_i}$  Eq. (14), and  
 613  $AMAK_{x_i}$  Eq. (16) associated with the critical pumping rate  $Q_c$  (25). Principal Sobol' indices,  $S_{x_i}$  Eq.  
 614 (7), are also listed;  $x_i = Pe_T, J, x_w$ .

	$AMAE_{x_i}$	$AMAV_{x_i}$	$S_{x_i}$	$AMAY_{x_i}$	$AMAK_{x_i}$
$Pe_T$	0.07	0.14	0.09	0.35	0.09
$J$	0.14	0.41	0.41	0.88	0.12
$x_w$	0.15	0.48	0.48	0.78	0.11

615

616

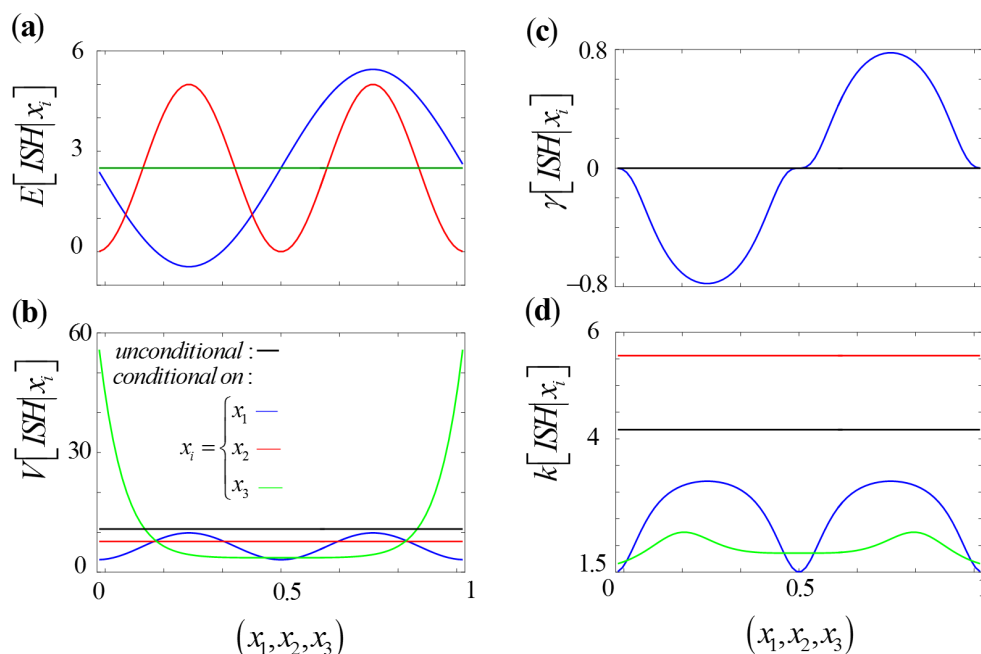


**Figure 1.** Variation of the first four moments of *ISH* Eq. (18) conditional to values of  $x_1$  (blue curves),  $x_2$  (red curves) and  $x_3$  (green curves) within the parameter space: (a) expected value,  $E[ISH | x_i]$ , (b) variance,  $V[ISH | x_i]$ , (c) skewness,  $\gamma[ISH | x_i]$ , and (d) kurtosis,  $k[ISH | x_i]$ , ( $i = 1, 2, 3$ ). The corresponding unconditional moments (black curves) are also depicted.

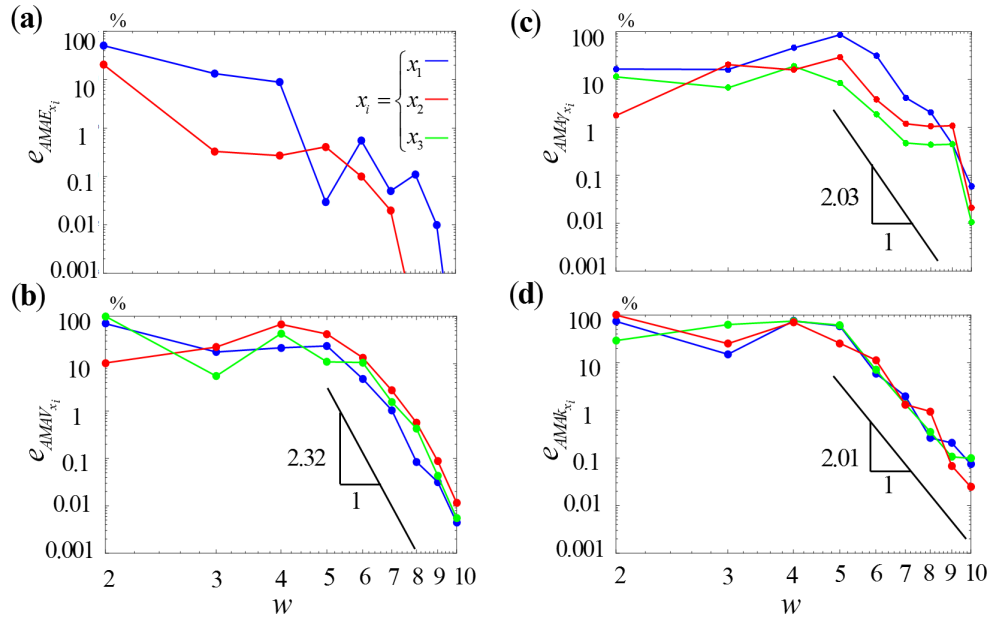
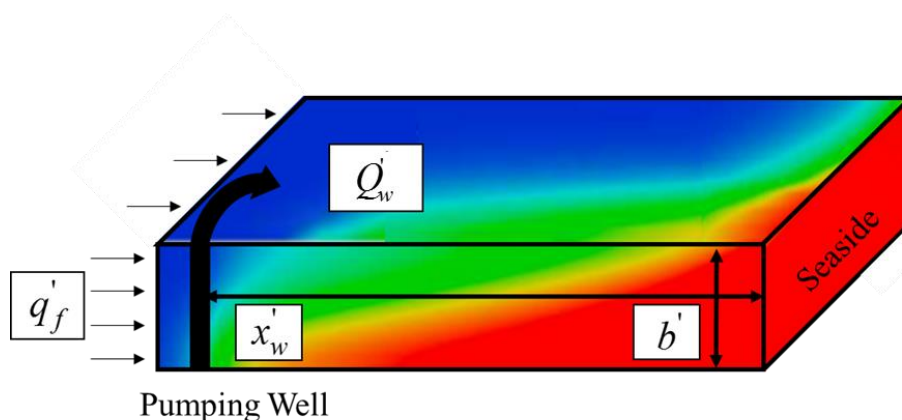


**Figure 2.** Error  $e_j$  Eq. (26) versus the total degree  $w$  of the gPCE representation of ISH for  $j =$  (a)  $AMAE_{x_i}$ , (b)  $AMAV_{x_i}$ , (c)  $AMA\gamma_{x_i}$  and (d)  $AMAk_{x_i}$ , with  $x_i = x_1$  (blue curves),  $x_2$  (red curves),  $x_3$  (green curves). Note that  $AMAE_{x_3}$  is always smaller than 0.001%. Average slope of the rate of decrease of  $e_j$  associated with the variance, skewness and kurtosis are indicated as a reference.





630

631 **Figure 3.** Sketch of the critical pumping scenario taking place within a coastal aquifer of thickness  
 632  $b'$ . A constant freshwater (in blue) flux,  $q_f'$ , flows from the inland to the coastline (saltwater in red).  
 633 A constant discharge,  $Q_w'$ , is pumped from a fully penetrating well located at a distance  $x_w'$  from the  
 634 coastline. Color scale indicating variable concentration of salt is only qualitative for illustration  
 635 purposes.

636

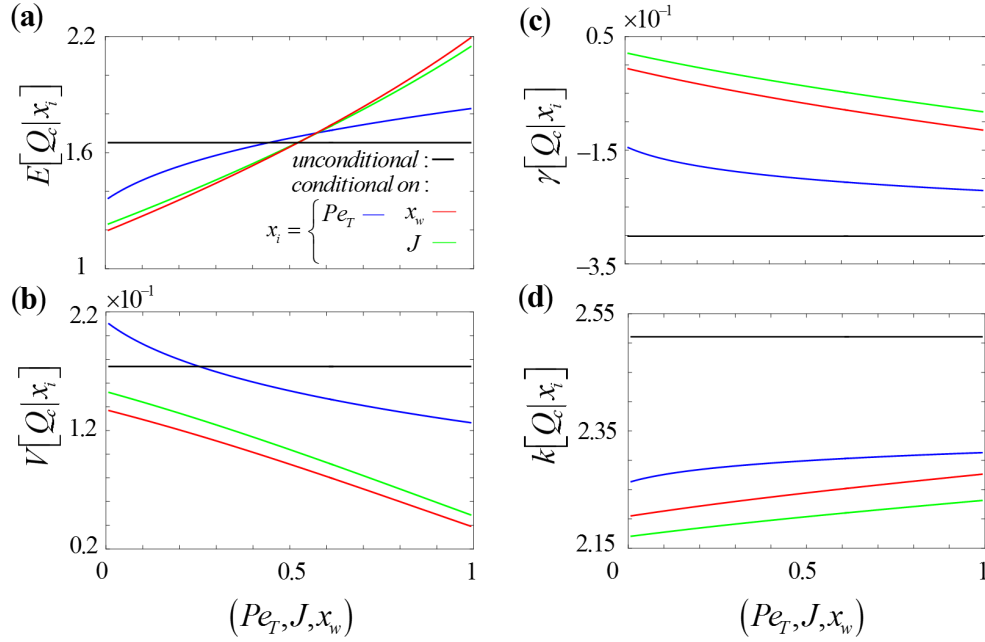


**Figure 4.** First four moments of  $Q_c$  Eq. (27) conditional to values of  $Pe_T$  (blue curves),  $J$  (green curves), and  $x_w$  (red curves) within the parameter space: (a) expected value,  $E[Q_c | x_i]$ , (b) variance,  $V[Q_c | x_i]$ , (c) skewness,  $\gamma[Q_c | x_i]$ , and (d) kurtosis,  $k[Q_c | x_i]$ , ( $x_i = Pe_T, J, x_w$ ). The corresponding unconditional moments (black curves) are also depicted. Intervals of variation of  $Pe_T$ ,  $J$  and  $x_w$  has been rescaled between zero and one for graphical representation purposes.

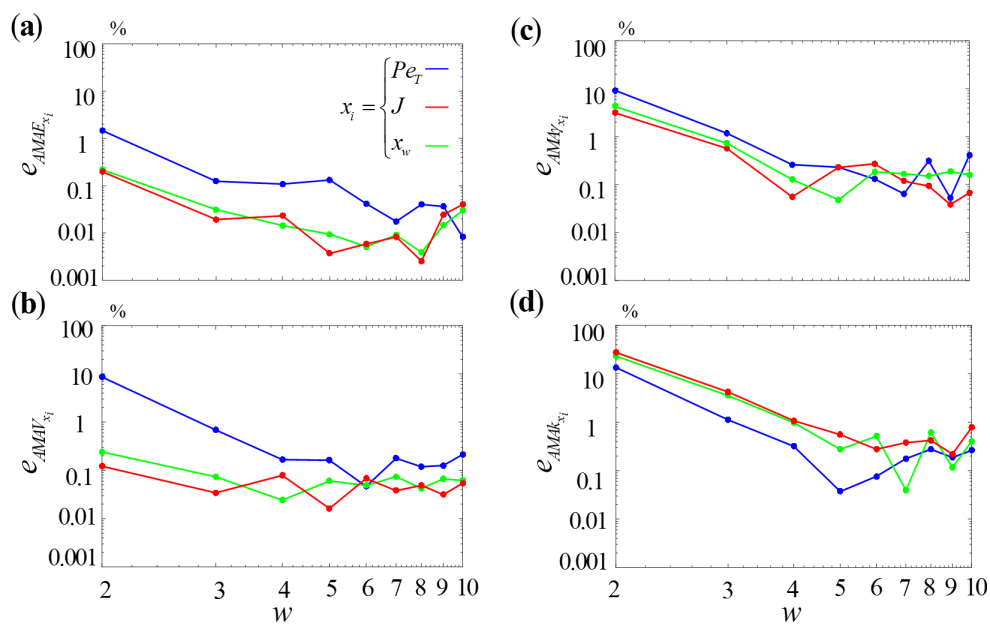


**Figure 5.** Error  $e_j$  Eq. (26) versus total degree  $w$  of the gPCE representation of  $Q_c$ , for  $j =$  (a)  $AMA E_{x_i}$ , (b)  $AMAV_{x_i}$ , (c)  $AMA\gamma_{x_i}$  and (d)  $AMAk_{x_i}$ ,  $x_i = Pe_T$  (blue curves),  $J$  (red curves),  $x_w$  (green curves).

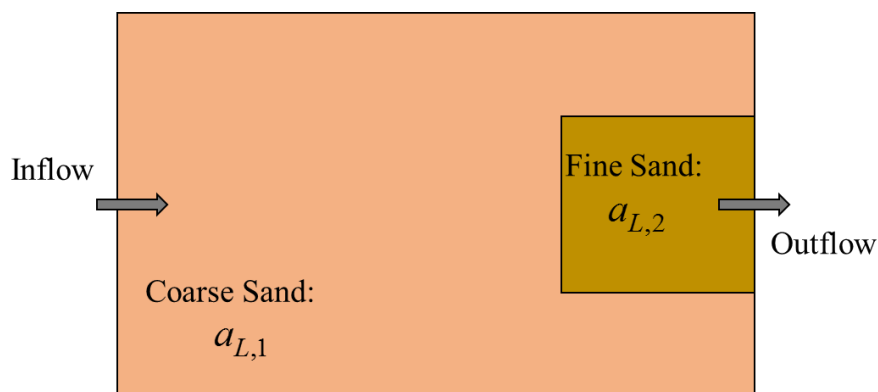


**Figure 6.** Sketch of the solute transport setting considered by Esfandiar et al. (2015).

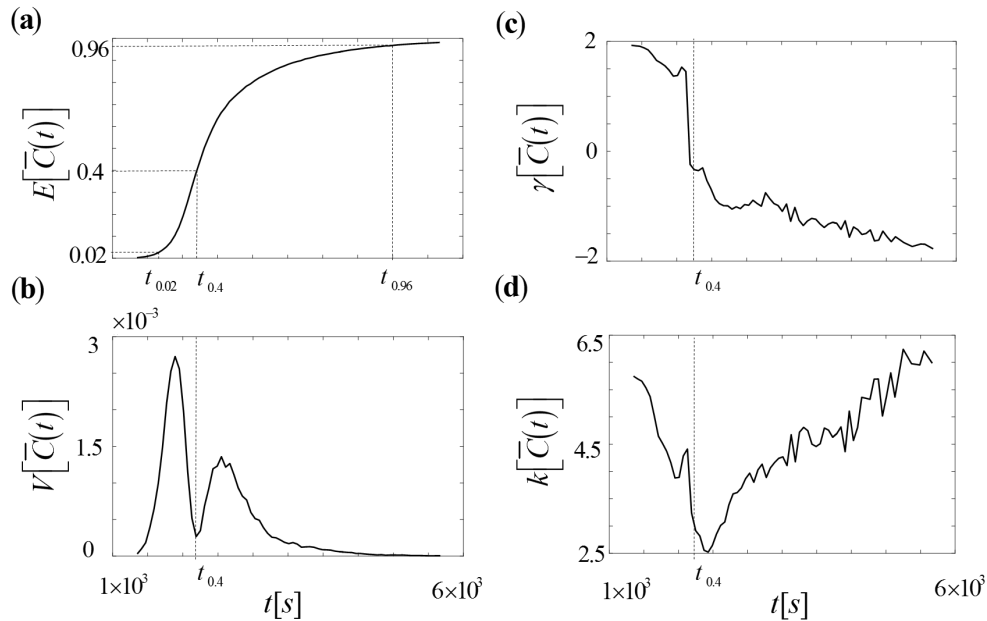


**Figure 7.** Temporal evolution of the unconditional (a) expected value,  $E[\bar{C}(t)]$ , (b) variance,  $V[\bar{C}(t)]$ , (c) skewness,  $\gamma[\bar{C}(t)]$ , and (d) kurtosis,  $k[\bar{C}(t)]$ , of normalized  $\bar{C}(t)$ . Vertical lines in (a) correspond to time steps  $t_{0.4}$ ,  $t_{0.02}$  and  $t_{0.96}$ , i.e., the times at which  $E[\bar{C}(t)] = 0.02, 0.4$ , and  $0.96$ , respectively.

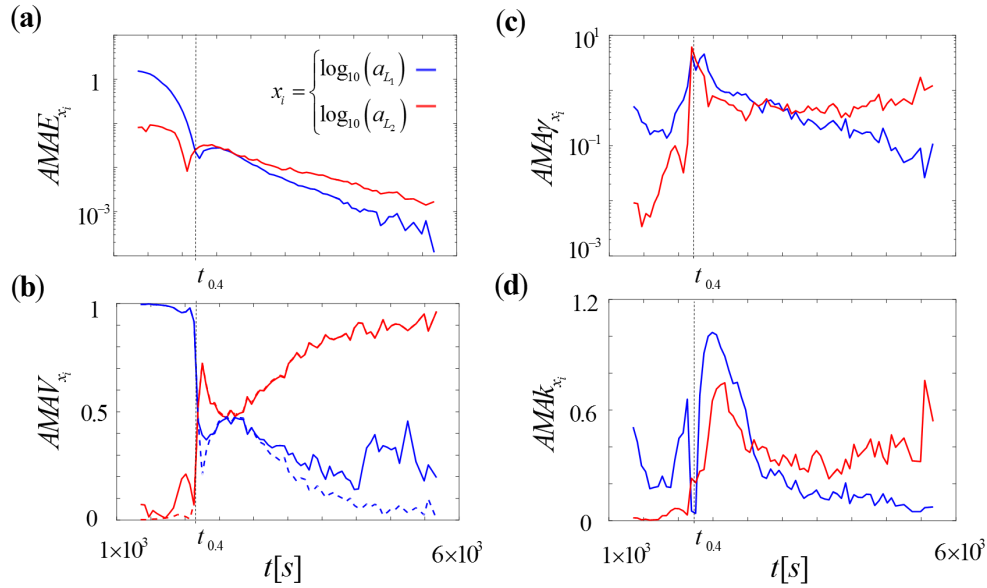


**Figure 8.** Time evolution of the global sensitivity index (a)  $AMAE_{x_i}$ , (b)  $AMAV_{x_i}$  and  $S_{x_i}$  (dashed curves), (c)  $AMA\gamma_{x_i}$ , and (d)  $AMAk_{x_i}$  of  $\bar{C}(t)$  ( $x_i = \log_{10}(a_{L,1})$  (blue), or  $\log_{10}(a_{L,2})$  (red)).

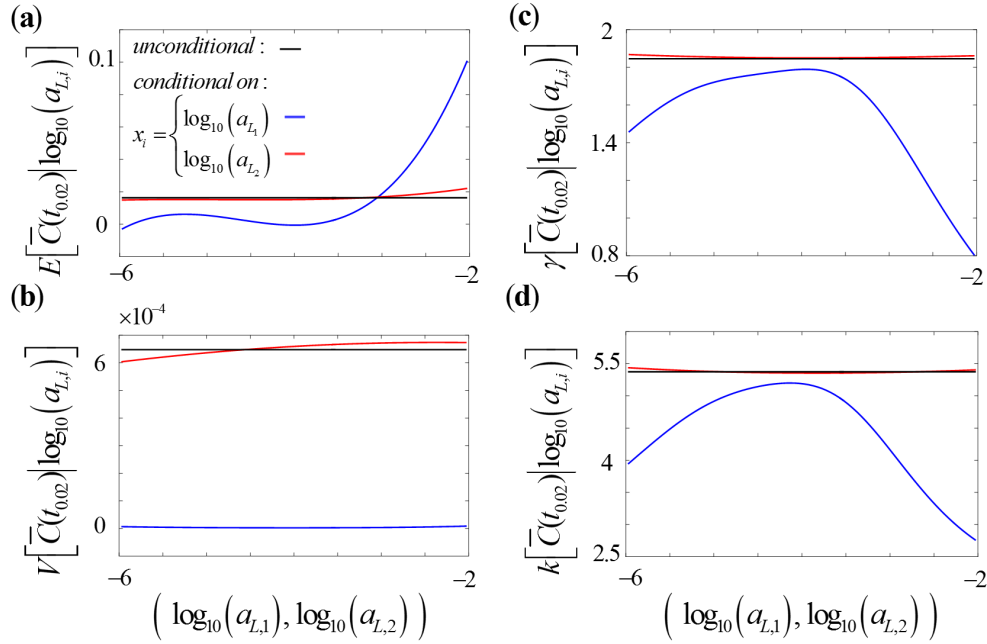


**Figure 9.** First four moments of  $\bar{C}(t=t_{0.02})$  conditional on  $\log_{10}(a_{L,1})$  (blue curves) and  $\log_{10}(a_{L,2})$  (red curves), at time  $t = t_{0.02}$ : (a) expected value,  $E[\bar{C}(t_{0.02})|\log_{10}(a_{L,i})]$ , (b) variance,  $V[\bar{C}(t_{0.02})|\log_{10}(a_{L,i})]$ , (c) skewness,  $\gamma[\bar{C}(t_{0.02})|\log_{10}(a_{L,i})]$ , and (d) kurtosis,  $k[\bar{C}(t_{0.02})|\log_{10}(a_{L,i})]$  ( $i = 1, 2$ ). The corresponding unconditional moments are also depicted (black curves).

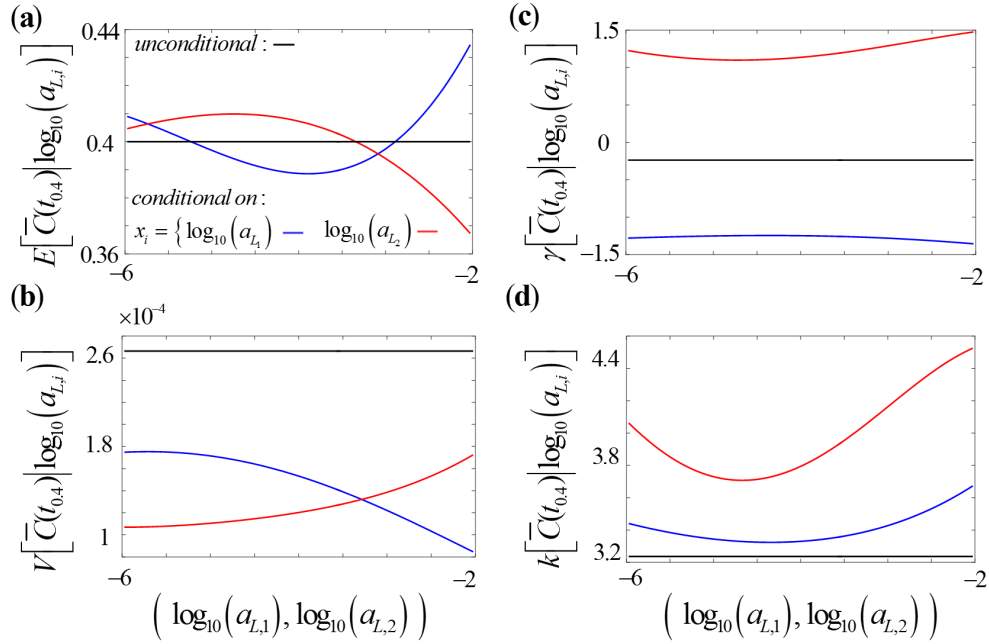
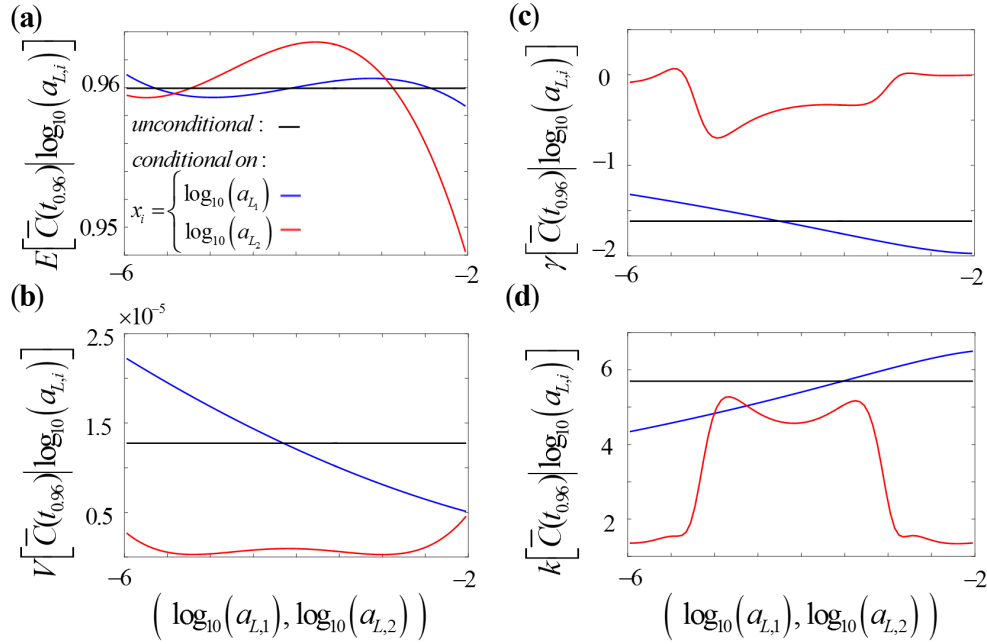


**Figure 10.** First four moments of  $\bar{C}(t=t_{0.4})$  conditional on  $\log_{10}(a_{L,1})$  (blue curves) and  $\log_{10}(a_{L,2})$  (red curves), at time  $t=t_{0.4}$ : (a) expected value,  $E[\bar{C}(t_{0.4})|\log_{10}(a_{L,i})]$ , (b) variance,  $V[\bar{C}(t_{0.4})|\log_{10}(a_{L,i})]$ , (c) skewness,  $\gamma[\bar{C}(t_{0.4})|\log_{10}(a_{L,i})]$ , and (d) kurtosis,  $k[\bar{C}(t_{0.4})|\log_{10}(a_{L,i})]$  ( $i=1, 2$ ). The corresponding unconditional moments are also depicted (black curves).





688

**Figure 11.** First four moments of  $\bar{C}(t=t_{0.96})$  conditional on  $\log_{10}(a_{L,1})$  (blue curves) and  $\log_{10}(a_{L,2})$  (red curves), at time  $t = t_{0.96}$ : (a) expected value,  $E[\bar{C}(t_{0.96})|\log_{10}(a_{L,i})]$ , (b) variance,  $V[\bar{C}(t_{0.96})|\log_{10}(a_{L,i})]$ , (c) skewness,  $\gamma[\bar{C}(t_{0.96})|\log_{10}(a_{L,i})]$ , and (d) kurtosis,  $k[\bar{C}(t_{0.96})|\log_{10}(a_{L,i})]$  ( $i = 1, 2$ ). The corresponding unconditional moments are also depicted (black curves).

694